Theor Chem Account (2009) 122:157–166
DOI 10.1007/s00214-008-0495-7

REGULAR ARTICLE

# A quantum mechanics study on the reaction mechanism of chalcone formation from *p*-coumaroyl-CoA and malonyl-CoA catalyzed by chalcone synthase

**Dai-lin Li · Qing-chuan Zheng · Hong-xing Zhang**

Received: 26 August 2008 / Accepted: 30 November 2008 / Published online: 16 December 2008


**Abstract** Chalcone synthase catalyzes formation of phenylpropanoid chalcone from one *p*-coumaroyl-coenzyme A (CoA) and three malonyl-CoA molecules. In order to elucidate structural and energetic features of the reaction mechanism, we performed the quantum mechanics calculations and obtained the following results. In loading step, only a tetrahedral intermediate is located without transition state (TS). Our results indicate that His303 acts as a $H_{31}$ donor, but not a hydrogen bond donor, to stabilize the intermediate formation. In decarboxylation step, the reaction proceeds via a TS and is sensitive to the environment. In elongation step, a tetrahedral TS is located. All of the results above support the reaction mechanism and further complement the proposal of Noel JP et al.

**Keywords** PKS · CHS · DFT · Reaction mechanism · TS

## 1 Introduction

Polyketide synthases (PKS) catalyze the biosynthesis of structurally diverse natural products in plants, fungi, and bacteria [1–3]. Many polyketide products possess pharmacological properties and are used as antibiotics, immunosuppressants, anti-cancer agents, and anti-fungal agents [4, 5]. Three types of PKS are known until now. Type I PKS are multifunctional enzymes which are organized into modules, each of which contains a set of distinct, non-iteratively acting activities for the catalysis of one cycle of polyketide chain elongation [6]. The main biosynthesis products of type I PKS are macrolides, polyethers, and polyene [6]. Type II PKS are multienzyme complexes that carry a single set of iteratively acting activities responsible for the biosynthesis of aromatic polyketides (often polycyclic) [6]. Type III PKS, also known as chalcone synthase (CHS) -like PKS, essentially are iteratively acting condensing enzymes responsible for biosynthesis of aromatic polyketides (often monocyclic or bicyclic) [6]. The CHS-like PKS are structurally and mechanistically the simplest PKS of the three types, which functions as homodimeric iterative PKS with two independent active sites that catalyzes a series of decarboxylation, condensation, and cyclization reactions [2, 3, 7, 8]. The best studied type III PKS is CHS, a plant-specific PKS, which uses *p*-coumaroyl-CoA as a starter molecule and three malonyl-CoA as extender molecules to form a tetraketide intermediate that is cyclized into 4,2′,4′,6′-tetrahydroxychalcone (chalcone) (Fig. 1a) [9]. The chalcone is essential for the biosynthesis of antimicrobial isoflavonoid phytoalexins, anthocyanin floral pigments, and flavonoid inducers of Rhizobium nodulation genes [10, 11]. Particularly, flavonoids are of interest as pharmacological agents and are constituents in plant-rich diets associated with a reduced risk of cardiovascular disease and some forms of cancer [12–16].

Due to the product diversity of biosynthesis intervened by chalcone, the studies on the reactions synthesizing chalcone are meaningful. Based upon experimental results, the roles of four conserved residues of CHS, Cys164, Phe215, His303 and Asn336, have been characterized during the formation of chalcone, and the reaction mechanism has been proposed which involves loading, decarboxylation, elongation (Fig. 1b), and cyclization steps

D.-l. Li · Q.-c. Zheng · H.-x. Zhang (✉)
State Key Laboratory of Theoretical and Computational Chemistry, Institute of Theoretical Chemistry, Jilin University, 130023 Changchun, People's Republic of China
e-mail: zhanghx@mail.jlu.edu.cn

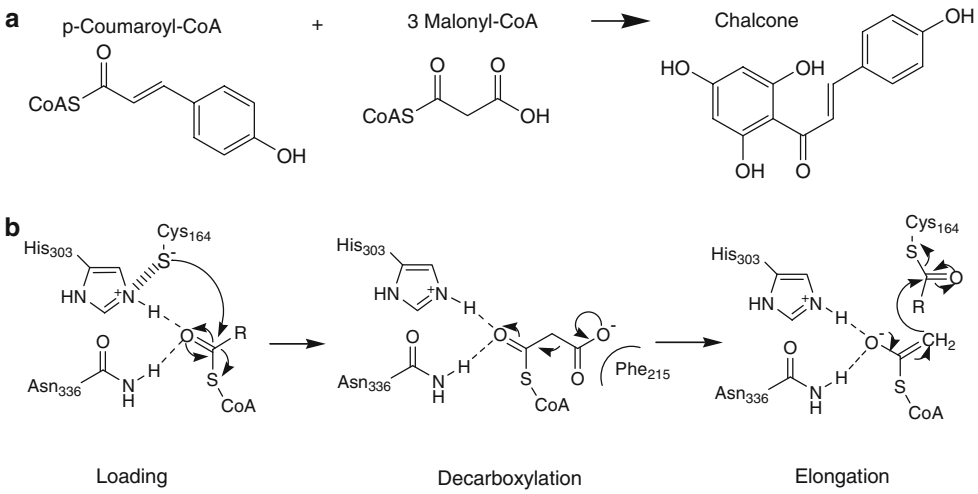


**Fig. 1** Reactions catalyzed by CHS: **a** overall reaction; **b** proposed reaction mechanism. Loading, decarboxylation, and elongation steps are shown. R is the coumaroyl moiety in the first cycle of the reaction and the cysteine-histidine ionic interaction in loading step is indicated [18, 19]

[17, 18]. In loading step, the thiolate of Cys164 attacks the thioester carbonyl carbon, and then the CoA moiety and sulfur atom dissociate from *p*-coumaroyl-CoA, leading to the transfer of the coumaroyl to Cys164. Besides forming a hydrogen bond with *p*-coumaroyl-CoA, His303 could interact with Cys164 through the interaction between N and S ion, which stabilizes the thiolate anion and induces the formation of the imidazolium-thiolate ion pair that plays a significant role in polyketide biosynthesis [17–20]. Asn336 stabilizes the tetrahedral intermediate formation through hydrogen bonds with *p*-coumaroyl-CoA in the step. In decarboxylation step, malonyl-CoA binds to the active site and orients the malonyl moiety to Phe215. The decarboxylation proceeds through a transition state (TS). His303 and Asn336, in the step, create an electron sink accommodating the negative charge by hydrogen bond interactions with malonyl-CoA, which potentially stabilize the TS. In elongation step, attack of the carbanion on the carbonyl carbon of the enzyme-bound thioester releases the thiolate anion of Cys164 and transfers the coumaroyl to the acetyl moiety of the CoA thioester, which results in the formation of the elongated diketide-CoA. Two hydrogen bonds from His303 and Asn336 could stabilize the tetrahedral TS. The three steps above accomplish the first cycle. Recapture of the elongated diketide-CoA by Cys164 and release of CoA initiate the second cycle. After three cycles, the tetraketide reaction intermediate will be formed and then cyclize by an intramolecular Claisen condensation into the product chalcone, a hydroxylated aromatic ring [17, 18].

Despite of extensive biochemical studies, to our best knowledge, theoretical studies on the formation of chalcone catalyzed by CHS, which can deeply characterize structural and energetic features of the reaction in electronic level, have not been reported yet. In the present study, quantum mechanics (QM) calculations on large chemical models from X-ray crystal structure were carried out to describe the reaction mechanism in the first cycle, including loading, decarboxylation, and elongation steps. A similar modeling approach has been used previously to investigate a number of other enzyme reaction mechanisms [21–25].

## 2 Computational method

The molecular simulations were performed on the SGI O3900 server using InsightII software package developed by Accelrys [26]. The consistent-valence forcefield (CVFF) was used for molecular docking and energy minimization. QM calculations were carried out using Gaussian 03 [27]. The Becke's three parameter functional and the Lee—Yang–Parr functional method with the 6-31G(d) basis set (B3LYP/6-31G(d)) was employed for the calculations of geometry optimization and frequency analysis [28–30].

### 2.1 Initial structure of the enzyme-substrate model in loading step

From the experimental geometries found in the Protein Data Bank (http://www.rcsb.org) for CHS, the structure (PDB code 1BQ6) with CoA as substrate was taken as the initial input. Since the substrate for our study was *p*-coumaroyl-CoA, the terminal sulfhydryl hydrogen atom of the inherent substrate CoA was replaced by coumaroyl in 1BQ6 with the aid of Builder module of InsightII software [26]. Affinity, a suite of programs for automatically docking a ligand to a receptor by a combination of Monte Carlo type and Simulated Annealing procedure, was used for docking *p*-coumaroyl-CoA to CHS and 100 steps energy minimization of conjugate

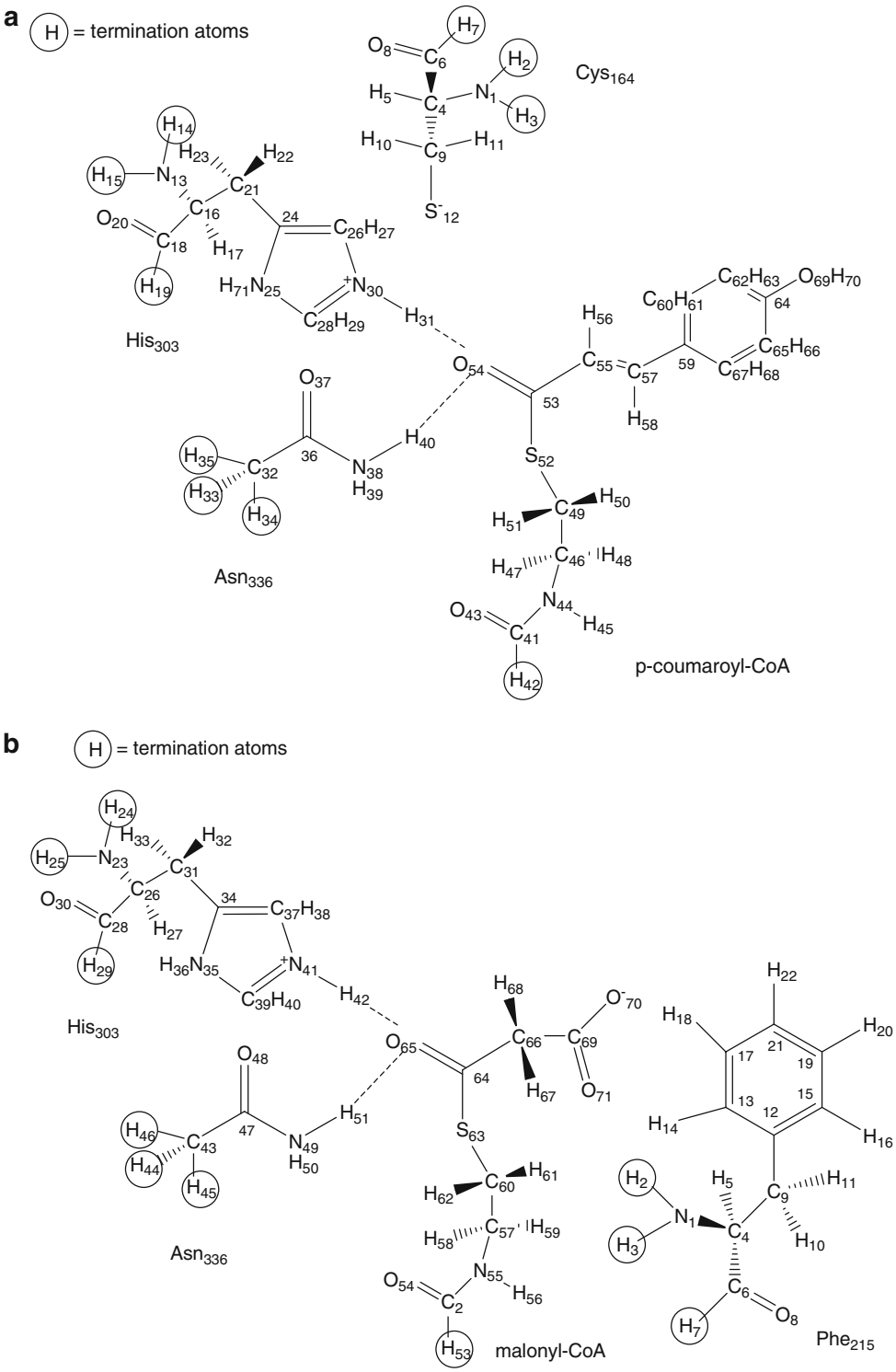


**Fig. 2** The initial CHS-substrate model of each step: **a** loading step; **b** decarboxylation step; **c** elongation step

gradient with a convergence value of 0.05 kcal $mol^{-1}$ $Å^{-1}$ was performed for the docked complex to release any internal strain in the structure [31]. To speed convergence of geometry optimization, the initial structure of loading step from the minimized geometry involves the whole of Cys164 and His303, the side chain of Asn336 plus $C_\alpha$ atom, and part of the substrate *p*-coumaroyl-CoA (Fig. 2a). Hydrogen termination atoms were added to satisfy the valencies of the border atoms. This 71-atom model was used to characterize the loading step. Based on the proposal that thiolate anion is present at physiological pH [19], the imidazolium-thiolate ion pair was employed artificially in our initial theoretical calculation model.

**Fig. 2** continued

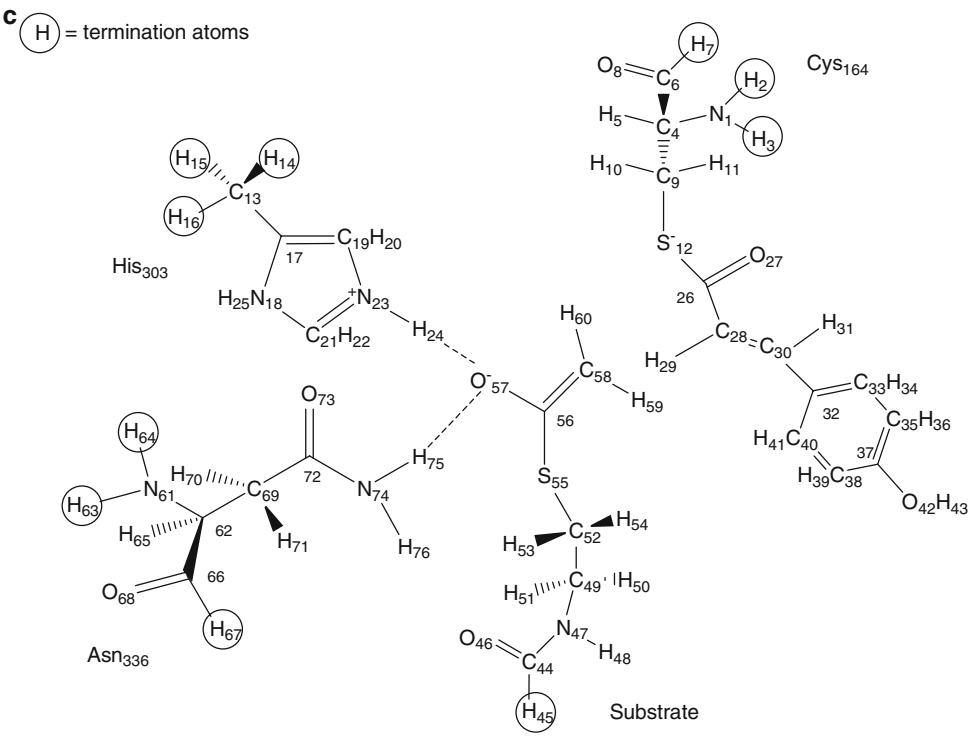


### 2.2 Initial structure of the enzyme-substrate model in decarboxylation step

As the substrate in the step was malonyl-CoA, we replaced the terminal sulfhydryl hydrogen atom of the inherent substrate CoA in 1BQ6 with malonyl and generated the CHS-malonyl-CoA complex by molecular docking [31]. An energy minimization of 100 steps of conjugate gradient with a convergence value of 0.05 kcal $mol^{-1}$ $Å^{-1}$ was then performed for CHS-malonyl-CoA complex. This 71-atom initial structure of decarboxylation step, which consists of the whole of Phe215 and His303, the side chain of Asn336 plus $C_\alpha$ atom, the malonyl-CoA substrate wherein the CoA moiety is the same as that in loading step, and hydrogen termination atoms (Fig. 2b), was used to elucidate the reaction property. Cys164 was not contained in the step as Cys164 is not essential for malonyl-CoA decarboxylation [18]. In addition, the Phe215 mutant experiments demonstrated that neither F215S nor F215Y significantly alters the $K_d$ for CoA or acetyl-CoA binding, but both dramatically alter the turnover rates for malonyl-CoA decarboxylation [18], meaning Phe215 plays an important role in decarboxylation step. Therefore, in our present study, Phe215 was only considered in decarboxylation step. In order to probe the role of Phe215 in further, the decarboxylation reactions of mutants, Phe215Tyr (F215Y) and Phe215Trp (F215 W), were also described, respectively. The models of mutants were obtained by the Builder module and refined by energy minimization [26].

### 2.3 Initial structure of the enzyme-substrate model in elongation step

To obtain the initial structure of elongation step, a molecular docking was performed on the complex formed by the modified CHS, where the thiolate of Cys164 was rebuilt to thioester with coumaroyl, and the substrate in which the coumaroyl moiety of *p*-coumaroyl-CoA was displaced with enol [31]. After 100 steps energy minimization of conjugate gradient with a convergence value of 0.05 kcal $mol^{-1}$ $Å^{-1}$, the initial structure of elongation step was intercepted from the minimized CHS-substrate complex. This 76-atom model, including the whole of Cys164 plus thioester and coumaroyl, the side chain of His303 plus $C_\alpha$ atom, the whole of Asn336, substrate, and hydrogen termination atoms (Fig. 2c), was used to describe the reaction process.

## 3 Results and discussions

### 3.1 The loading step

In order to theoretically characterize the loading step in detail, we constructed the 71-atom model as mentioned above (Fig. 2a) and carried out the QM calculations to scan the potential energy surface (PES) with a range of $S_{12}$–$C_{53}$ (2.50–1.90 Å) and $S_{52}$–$C_{53}$ (1.90–2.90 Å) distances in 0.1-Å steps. In total 77 structures were generated, in which all

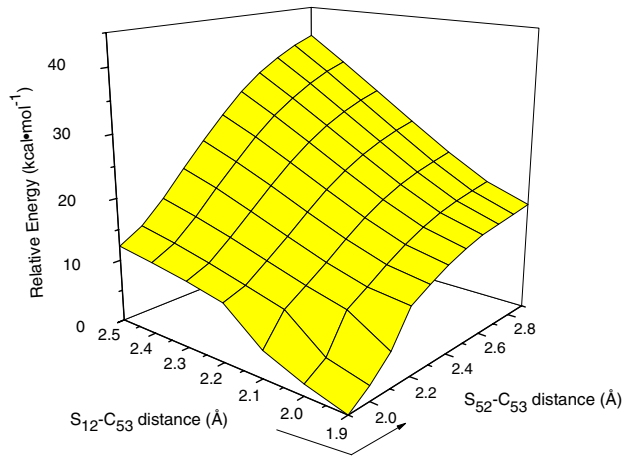


**Fig. 3** Potential energy surface in loading step (Energy of the structure D ($S_{12}$–$C_{53}$) = 1.90 Å and D ($S_{52}$–$C_{53}$) = 1.90 Å was taken as zero)

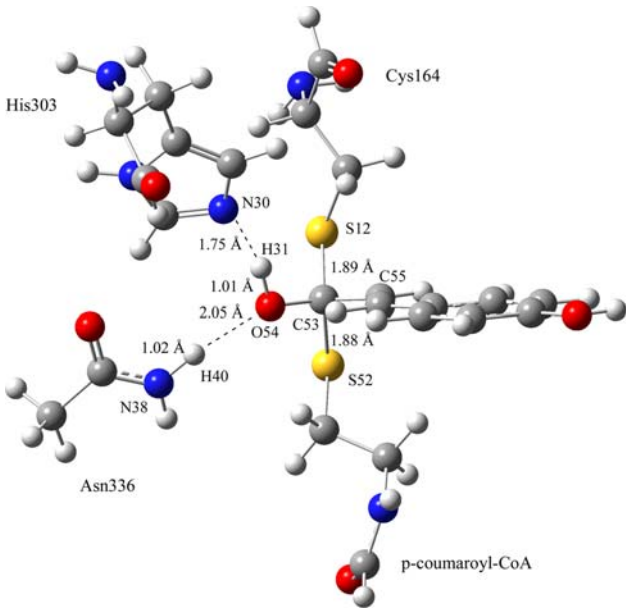


**Fig. 4** Structures of intermediates obtained through optimization with only hydrogen termination atoms fixed in loading step

geometric parameters, except for $S_{12}$–$C_{53}$ and $S_{52}$–$C_{53}$ lengths, were optimized with six hydrogen termination atoms ($H_7$, $H_{14}$, $H_{15}$, $H_{33}$, $H_{34}$, $H_{35}$) frozen at the original positions.

The PES of loading step, based on the scan results, is shown in Fig. 3. It is clear that the reaction proceeds via an intermediate without TS for none of first order saddle point is located on the PES. At the beginning of the step, the $S_{12}$ anion attacks the carbonyl $C_{53}$ atom. As the distance between them decreases gradually, the total energy of the reaction also decreases accordingly until the intermediate is formed which is the point with lowest energy on PES, D ($S_{12}$–$C_{53}$) = 1.90 Å and D ($S_{52}$–$C_{53}$) = 1.90 Å (Fig. 3). After the intermediate formation, the $S_{52}$ atom with CoA moiety dissociates from *p*-coumaroyl-CoA which means the distance between $S_{52}$ and $C_{53}$ atom increases overcoming the energy disadvantage. This is the minimum energy reaction path from reactants to products. As a mere stationary point on the reaction path, the intermediate structure extraordinarily interests us. Due to the optimization with fixed $S_{12}$–$C_{53}$ and $S_{52}$–$C_{53}$ distances, the structure obtained from the PES scan may differ from the real that the intermediate ought to have. To get the real structure of the intermediate, the optimization with only hydrogen termination atoms fixed was done and frequency calculation was then carried out to verify the rationality of the optimized structure. Figure 4 shows the optimized geometry without any imaginary frequency. The intermediate adopts the tetrahedral geometry with little distortion, in which three angles of $O_{54}$–$C_{53}$–$S_{12}$, $O_{54}$–$C_{53}$–$C_{55}$, and $O_{54}$–$C_{53}$–$S_{52}$ are 113.15°, 113.40°, and 107.99°, respectively which are close to that of standard tetrahedral configuration (109.50°) (Figs. 2a, 4). The $S_{12}$–$C_{53}$ and $S_{52}$–$C_{53}$ distances, 1.89 and 1.88 Å for, respectively, are both close to the original distance 1.90 Å. The bond distance similarity confirms the rationality of our PES scan.

**Table 1** The charges of residues and *p*-coumaroyl-CoA in Reactants and Intermediate of loading step with the change of them (Q/e)

| | Reactants | Intermediate | Change |
|---|---|---|---|
| Cys164 | −0.452 | 0.042 | 0.494 |
| His303 | 0.784 | 0.516 | −0.268 |
| Asn336 | 0.004 | 0.012 | 0.008 |
| *p*-coumaroyl-CoA | −0.336 | −0.570 | −0.234 |

Atomic charge analysis, reflecting the electron transfer to reveal the roles of residues during the reaction, was performed. Table 1 lists the charges determined by Mulliken population analysis in reactants and intermediate with the change of them. The charge of each residue or the substrate is the summation of atomic charge of all of the constituent atoms. It is clear that the charges of Cys164 and Asn336 increase which means the lost of electrons, however the charges of His303 and substrate *p*-coumaroyl-CoA decrease which means the gain of electrons (Table 1). The charge increase of Cys164 (0.494 Q/e) is more than the decrease of *p*-coumaroyl-CoA (0.234 Q/e), indicating that the electrons of Cys164 have transferred not only to the substrate *p*-coumaroyl-CoA, but also to the electron-gained residue, His303, which means the $S_{12}$–$C_{53}$ bond has been formed and the interaction between Cys164 and His303 does exist. Our theoretical deduction from atomic charge analysis supports the proposal, that an imidazolium–

thiolate ion pair is present through the interaction between Cys164 and His303 [17–19].

Besides interacting with Cys164, His303 was proposed to act a hydrogen bond donor towards $O_{54}$, stabilizing the formation of the tetrahedral intermediate [20]. In the present study, our results indicate His303 could indeed stabilize the intermediate formation, however, not through the hydrogen bond with *p*-coumaroyl-CoA, but break of the $N_{30}$–$H_{31}$ bond to form the $H_{31}$–$O_{54}$ bond. The distances of $N_{30}$–$H_{31}$ and $H_{31}$–$O_{54}$ have changed from 1.06 to 1.60 Å in reactants (data not shown) to 1.75 and 1.01 Å in intermediate (Fig. 4) respectively, which means $H_{31}$ atom have transferred from $N_{30}$ to $O_{54}$ with break of the $N_{30}$–$H_{31}$ bond and formation of the $H_{31}$–$O_{54}$. This may result from the increased negative charge of $O_{54}$. The charge of $O_{54}$ is −0.573 Q/e in reactants while −0.652 Q/e in intermediate, implying 0.079 Q/e negative charge increase (data not shown). The negative charge increase induces the enhanced electrostatic interaction between $H_{31}$ and $O_{54}$ thus ultimately result in the $H_{31}$ transfer from His303 to *p*-coumaroyl-CoA. It is the $H_{31}$–$O_{54}$ bond formation that neutralizes the increased negative charge of $O_{54}$ and further stabilizes the tetrahedral intermediate formation. After that, with the elongation of $S_{52}$–$C_{53}$ distance, the negative charge of $O_{54}$ decreases gradually, thus $H_{31}$ atom starts to transfer from $O_{54}$ to $N_{30}$ under the attraction from $N_{30}$ and bonds to $N_{30}$ in the product of the step. Therefore, we think His303 acts as a $H_{31}$ donor through break of the $N_{30}$–$H_{31}$ bond to stabilize the intermediate formation in loading step. Furthermore, Asn336 stabilizes the intermediate formation through hydrogen bond, with the $H_{40}$–$O_{54}$ distance 2.05 Å (Fig. 4).

### 3.2 The decarboxylation step

The next reaction step to be studied is decarboxylation of malonyl-CoA. To investigate the decarboxylation reaction path, a potential energy curve (PEC) scan was performed for a range of fixed $C_{66}$–$C_{69}$ distances from 1.6 to 2.8 Å in 0.1-Å step on the 71-atom model built above (Fig. 2b). Thus a series of 13 structures was generated, in which all geometric parameters of the model, except for the $C_{66}$–$C_{69}$ bond length, were optimized with seven hydrogen termination atoms ($H_7$, $H_{24}$, $H_{25}$, $H_{44}$, $H_{45}$, $H_{46}$, $H_{53}$) frozen at the original positions.

The PEC based on the scan results is shown in Fig. 5a. It can be seen that the energy increases during the elongation of $C_{66}$–$C_{69}$ distance from 1.70 to 2.30 Å and decreases from 2.30 to 2.80 Å. Therefore the TS is thought to be around 2.30 Å and a finer PEC scan is performed with the $C_{66}$–$C_{69}$ distance ranging from 2.20 to 2.40 Å in 0.02-Å step. The maximum energy appears at 2.36 Å of the $C_{66}$–$C_{69}$ distance in the finer PEC scan (data not shown). This

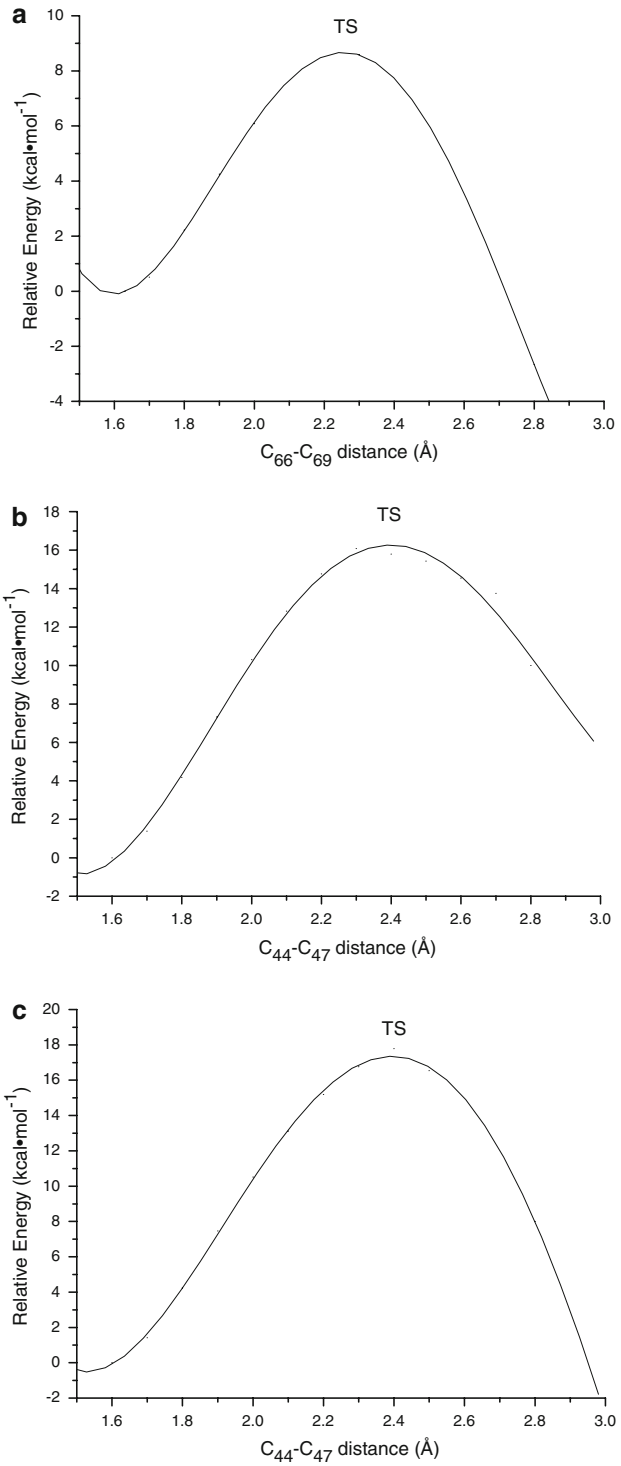


**Fig. 5** Potential energy curve in decarboxylation step for CHS, F215Y and F215 W, respectively: **a** CHS (Energy of the structure D ($C_{66}$–$C_{69}$) = 1.63 Å was taken as zero); **b** F215Y (Energy of the structure D ($C_{44}$–$C_{47}$) = 1.60 Å was taken as zero); **c** F215 W (Energy of the structure D ($C_{44}$–$C_{47}$) = 1.60 Å was taken as zero)

structure is subsequently refined and confirmed to be a TS by the frequency analysis for only one imaginary frequency exists. The structure of TS is described in Fig. 6, together

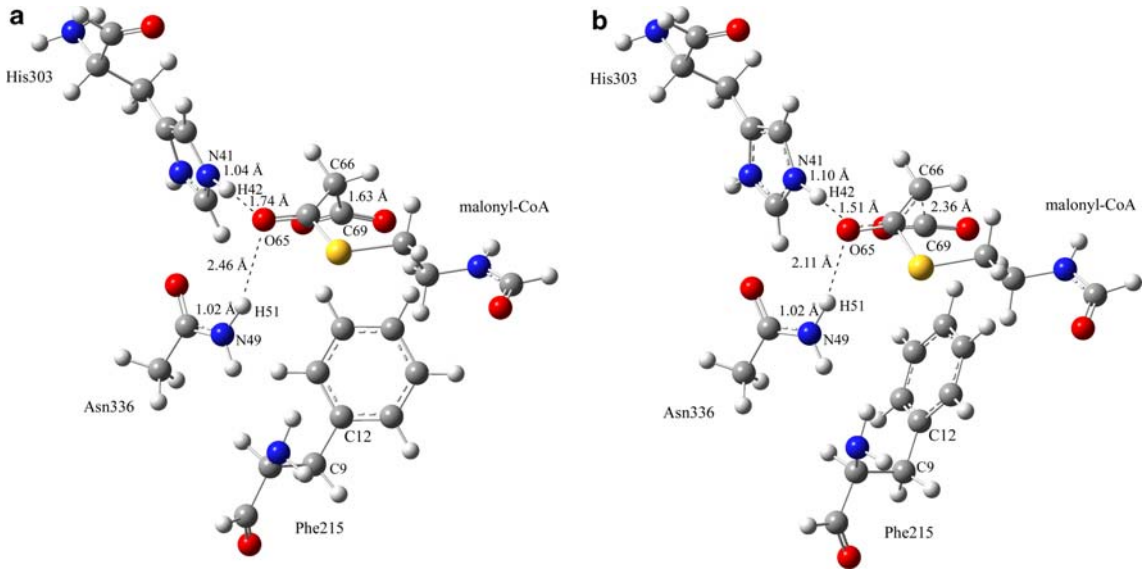


**Fig. 6** Structures of reactants and TS for CHS in decarboxylation step: **a** reactants; **b** TS

**Table 2** The charges of residues, malonyl-CoA (not include $CO_2$), and $CO_2$ in Reactants and TS of decarboxylation step with the change of them: (a) CHS; (b) F215Y; (c) F215 W (Q/e)

| | Reactants | TS | Change |
|---|---|---|---|
| (a) | | | |
| Phe215 | −0.054 | −0.009 | 0.045 |
| His303 | 0.830 | 0.778 | −0.052 |
| Asn336 | −0.001 | −0.009 | −0.008 |
| Malonyl-CoA | −0.229 | −0.580 | −0.351 |
| $CO_2$ | −0.546 | −0.180 | 0.366 |
| (b) | | | |
| Tyr215 | −0.083 | −0.037 | 0.046 |
| His303 | 0.818 | 0.761 | −0.057 |
| Asn336 | −0.025 | 0.008 | 0.033 |
| Malonyl-CoA | −0.165 | −0.575 | −0.410 |
| $CO_2$ | −0.545 | −0.157 | 0.388 |
| (c) | | | |
| Trp215 | −0.084 | −0.001 | 0.083 |
| His303 | 0.829 | 0.727 | −0.102 |
| Asn336 | 0.006 | 0.022 | 0.016 |
| Malonyl-CoA | −0.191 | −0.616 | −0.425 |
| $CO_2$ | −0.560 | −0.132 | 0.428 |

with that of reactants. During the formation of TS, the configuration of Phe215 changes mostly, referring to the rotation of benzene ring around the $C_9$–$C_{12}$ bond, which happens at 2.24 Å of the $C_{66}$–$C_{69}$ distance (Fig. 6).

The roles of residues involved in the TS formation were described based on the geometries of reactants and TS, and the atomic charge analysis determined by Mulliken population. The charge of Phe215 changes from −0.054 Q/e in reactants to −0.009 Q/e in TS (Table 2a), which means Phe215 is nearly neutral in TS and could provides a non-polar environment for the decarboxylation of malonyl-CoA. The distances of $N_{41}$–$H_{42}$ and $H_{42}$–$O_{65}$ have changed from 1.04 and 1.74 Å in reactants to 1.10 and 1.51 Å, respectively (Fig. 6) caused by the negative charge increase of $O_{65}$, from −0.495 Q/e to −0.623 Q/e (data not shown), implying the hydrogen bond interaction between $H_{42}$ and $O_{65}$ has been enhanced. The enhanced hydrogen bond interaction also happens between $H_{51}$ and $O_{65}$ for the decreased distance, from 2.46 Å in reactants to 2.11 Å in TS. Therefore, His303 and Asn336 both stabilize the developing negative charge via hydrogen bond interactions with thioester carbonyl $O_{65}$ of malonyl-CoA during the TS formation (Fig. 6).

To probe the role of Phe215 in further, the F215Y and F215 W mutants were modeled for the decarboxylation reaction calculations respectively. The PEC scans were performed, respectively, to locate TS of each mutant in the same method as that used in CHS. The scan results were shown in Fig. 5. After that, the Mulliken population analyses were carried out again for each mutant (Table 2b, c).

It can be seen that the energy decreases at 2.30 Å in F215Y and at 2.40 Å in F215 W (Fig. 5b and 5c). Thus the structures around were used for locating TS. Figure 7 lists the TS structure for each mutant respectively in the step. In TS of F215Y, the $C_{44}$–$C_{47}$ bond distance is 2.36 Å, which is the same as $C_{66}$–$C_{69}$ bond distance in CHS, while TS of F215 W happens later at 2.45 Å of $C_{44}$–$C_{47}$ bond distance. The energy barriers (ΔE), which were calculated by means of $\Delta E = E$ (TS) $- E$ (Reactants) with zero point energy (ZPE) correction, are 5.5, 12.7, and 13.2 kcal mol$^{-1}$ for CHS, F215Y, and F215 W, respectively, meaning

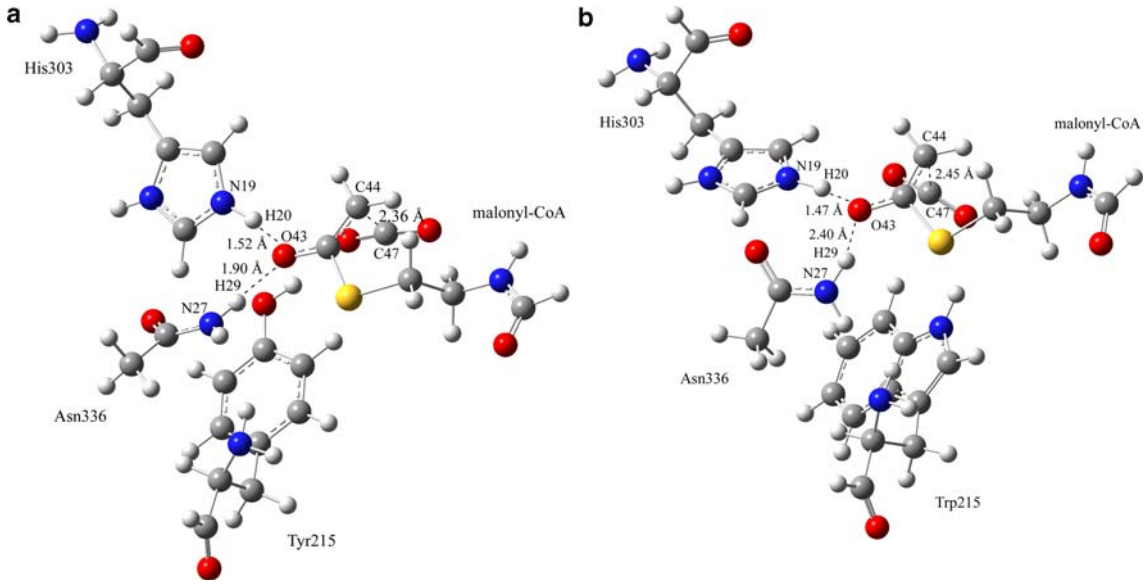


**Fig. 7** Structures of TS for mutants in decarboxylation step: **a** F215Y; **b** F215 W

that the decarboxylation reactions proceed via increased energy barriers, thus leading to the reaction activity in CHS > F215Y > F215 W order. The reaction activity order from our theoretical calculation accords well with that of the kinetic parameters obtained by Noel JP et al., which is F215Y and F215 W mutants retain decarboxylation activity but with 80 and 450-fold reductions compared to CHS for the decarboxylation reaction respectively [18]. The consistency of the activity order validates the rationality of our model.

What have caused the decreased activity of each mutant? In F215Y, the distances of $H_{20}$–$O_{43}$ and $H_{29}$–$O_{43}$ are 1.52 and 1.90 Å, respectively, in TS (Fig. 7a), indicating two hydrogen bonds are formed and thus His303 and Asn336 function in the same way as that of CHS in the step. In F215 W, the distances of $H_{20}$–$O_{43}$ and $H_{29}$–$O_{43}$ 1.47 and 2.40 Å, respectively in TS (Fig. 7b), also indicate His303 and Asn336 play the same role as that of CHS. It is hence evident that the decreased activity of decarboxylation of malonyl-CoA arises from the role of residue215. As proposed by O'Leary MH that the conversion of a carboxylate group, which is polar and charged, into carbon dioxide, which is nonpolar and uncharged, is sensitive to environment [32], thus the environment in the step attracts our attention. Through the atomic charge analyses, we found that two aspects are essential for the malonyl-CoA decarboxylation: one is the nonpolar environment, the other is the change in environment. It can be seen that the charge changes of Phe215 and Tyr215, 0.045 Q/e and 0.046 Q/e, respectively (Table 2a, b), are nearly the same, meaning the changes in the environment that residue215 induces are nearly the same. Under the condition of that, we infer that the nonpolar environment is important for the decarboxylation, because Phe215 could provide more nonpolar environment compared to Tyr215 both in reactants and in TS, leading to the higher activity of CHS. Furthermore, the charge change of Trp215 (0.083 Q/e) is much larger than that of Tyr215 (0.046 Q/e), (Table 2b, c), indicating the change in environment in F215 W is larger than that in F215Y. Though Trp215 could provide more nonpolar environment due to the less charge in TS compared to Tyr215 (Table 2b, c), F215 W is still less active than F215Y. Therefore, we infer that the change in environment is more important than the nonpolar environment in the case of large differences of the environmental changes. In conclusion, the environmental change plays a dominant role for the malonyl-CoA decarboxylation; however, under the condition of similar environmental changes, the nonpolar environment is critical.

### 3.3 The elongation step

To investigate the features of the reaction path, a PEC scan was performed for a range of fixed $C_{26}$–$C_{58}$ distances from 1.7 to 2.7 Å in 0.1-Å step on the 76-atom model constructed above (Fig. 2c). Therefore, 11 structures were generated in total, in which all geometric parameters of the model, except for the $C_{26}$–$C_{58}$ bond length, were optimized with four hydrogen termination atoms ($H_7$, $H_{16}$, $H_{45}$, $H_{67}$) frozen at the original positions.

As shown in Fig. 8, we can see that the maximum energy point, which is thought to be a TS, appears at 1.90 Å of $C_{26}$–$C_{58}$ distance. This structure is subsequently optimized and verified to be a TS by the frequency

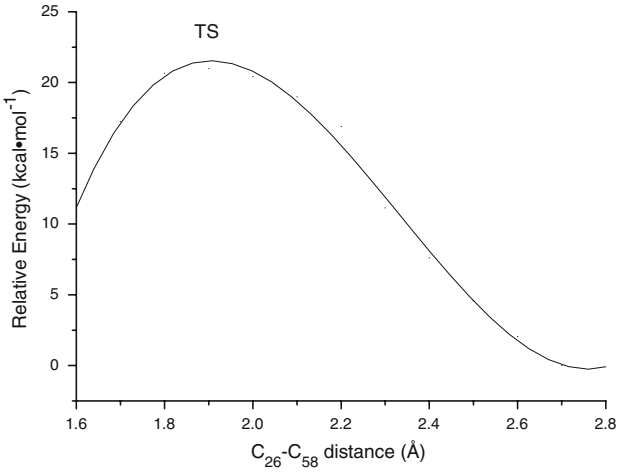


**Fig. 8** Potential energy curve in elongation step (Energy of the structure D ($C_{26}$–$C_{58}$) = 2.70 Å was taken as zero)

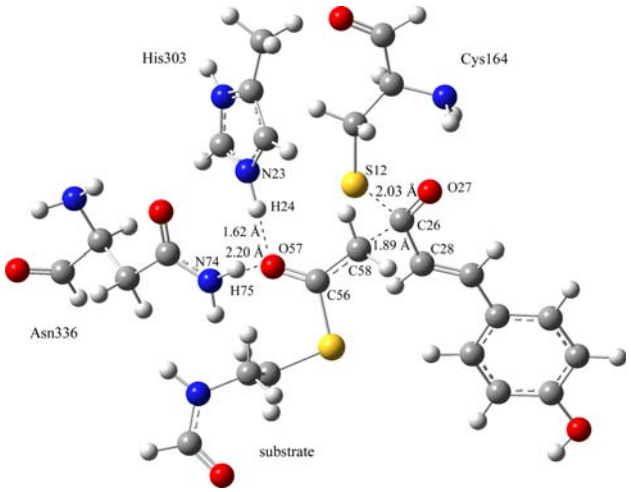


**Fig. 9** Structure of TS for CHS in elongation step

calculation result that only one imaginary frequency exists. The distances of $C_{26}$–$C_{58}$ and $S_{12}$–$C_{26}$ in TS are 1.89 and 2.03 Å, respectively (Fig. 9). The three bond angles of $C_{58}$–$C_{26}$–$S_{12}$, $C_{58}$–$C_{26}$–$O_{27}$, and $C_{58}$–$C_{26}$–$C_{28}$ are 104.31°, 104.15°, and 104.98°, respectively, indicating that the TS adopts tetrahedral geometry with little distortion. Moreover, two hydrogen bonds, which could stabilize the TS formation, are formed between $H_{24}$ and $O_{57}$ atoms and $H_{75}$ and $O_{57}$ atoms with the distances 1.62 and 2.20 Å for respective (Fig. 9). The results indicate His303 and Asn336 both act as a hydrogen bond donor in the step.

## 4 Conclusions

The QM calculations were carried out to characterize loading, decarboxylation, and elongation steps in the first cycle of CHS catalytic reactions at the level of B3LYP/6-31G(d). In loading step, the reaction proceeds via a tetrahedral intermediate without TS for none of first order saddle point is located on the basis of PES scan. Atomic charge analysis confirmed the interaction between Cys164 and His303 and indicates that His303 acts as a $H_{31}$ donor through break of the $N_{30}$–$H_{31}$ bond, but not a hydrogen bond donor, to stabilize the intermediate formation. Asn336 forms a hydrogen bond between $H_{40}$ and $O_{54}$ to stabilize the intermediate. In decarboxylation step, the reaction proceeds via a TS, in which the TS happens at 2.36 Å of $C_{66–69}$ bond. His303 and Asn336 form hydrogen bonds with thioester carbonyl $O_{65}$ of malonyl-CoA that stabilize the developing negative charge. In order to probe the role of Phe215 in further, F215Y and F215 W mutants were modeled for decarboxylation reaction calculations, respectively. The TS of each mutant happens at 2.36 and 2.45 Å of $C_{44}$–$C_{47}$ bond, respectively. The calculated reaction energy barriers are 5.5, 12.7, and 13.2 kcal mol$^{-1}$ for CHS, F215Y, and F215 W respectively, which means the reaction activity is in CHS > F215Y > F215 W order, corresponding well to that on experiments [18]. Through the charge analyses for Phe215, Tyr215, and Trp215, we found the environmental change plays a dominant role for the malonyl-CoA decarboxylation; however, under the condition of similar environmental changes, the nonpolar environment is critical. In elongation step, the reaction proceeds via a tetrahedral TS, in which the distances of $C_{26}$–$C_{58}$ and $S_{12}$–$C_{26}$ are 1.89 and 2.03 Å, respectively. All of the theoretical results could support the reaction mechanism and further complement the proposal of Noel et al.

**Acknowledgments** This work was supported by the Natural Science Foundation of China, Key Projects in the National Science and Technology Pillar Program, and Specialized Research Fund for the Doctoral Program of Higher Education (grant no. 20573042, 2006BAE03B01, and 20070183046).

## References

1. Hopwood DA, Sherman DH (1990) Annu Rev Genet 23:37–66. doi:10.1146/annurev.ge.24.120190.000345
2. Schroder J (1997) Trends Plant Sci 2:373–378. doi:10.1016/S1360-1385(97)87121-X
3. Shen B (2000) Top Curr Chem 209:1–51. doi:10.1007/3-540-48146-X_1
4. Hutchinson CR (1998) Curr Opin Microbiol 1:319–329. doi:10.1016/S1369-5274(98)80036-2
5. Bentley R, Bennett JW (1999) Annu Rev Microbiol 53:411–446. doi:10.1146/annurev.micro.53.1.411
6. Shen B (2003) Curr Opin Chem Biol 7:285–295. doi:10.1016/S1367-5931(03)00020-6
7. Shen B, Hutchinson CR (1993) Science 262:1535–1540. doi:10.1126/science.8248801
8. Tropf S, Karcher B, Schroder G, Schroder J (1995) J Biol Chem 270:7922–7928. doi:10.1074/jbc.270.14.7922

9. Kreuzaler F, Hahlbrock K (1975) Eur J Biochem 56:205–213. doi:10.1111/j.1432-1033.1975.tb02223.x
10. Dixon RA, Paiva NL (1995) Plant Cell 7:1085–1097
11. Long SR (1989) Cell 56:203–214. doi:10.1016/0092-8674(89)90893-3
12. Edwards ML, Stemerick DM, Sunkara PS (1990) J Med Chem 33:1948–1954. doi:10.1021/jm00169a021
13. Li R, Kenyon GL, Cohen FE, Chen X, Gong B, Dominguez JN, Davidson E, Kurzban G, Miller RE, Nuzum EO, Rosenthal PJ, Mckerrow JH (1995) J Med Chem 38:5031–5037. doi:10.1021/jm00026a010
14. Zwaagstra ME, Timmerman H, Tamura M, Tohma T, Wada Y, Onogi K, Zhang MQ (1997) J Med Chem 40:1075–1089. doi:10.1021/jm960628d
15. Birt DF, Pelling JC, Nair S, Lepley D (1996) Prog Clin Biol Res 395:223–234
16. Setchell KD, Cassidy A (1999) J Nutr 129:758S–767S
17. Ferrer JL, Jez JM, Bowman ME, Dixon RA, Noel JP (1999) Nat Struct Biol 6:775–784. doi:10.1038/11553
18. Jez JM, Ferrer JL, Bowman ME, Dixon RA, Noel JP (2000) Biochemistry 39:890–902. doi:10.1021/bi991489f
19. Jez JM, Noel JP (2000) J Biol Chem 275:39640–39646. doi:10.1074/jbc.M008569200
20. Jez JM, Ferrer JL, Bowman ME, Austin MB, Schroder J, Dixon RA, Noel JP (2001) J Ind Microbiol Biotechnol 27:393–398. doi:10.1038/sj.jim.7000188
21. Robinet JJ, Cho KB, Gauld JW (2008) J Am Chem Soc 130:3328–3334. doi:10.1021/ja072650+
22. Robinet JJ, Gauld JW (2008) J Phys Chem B 112:3462–3469. doi:10.1021/jp075415m
23. Chen SL, Marino T, Fang WH, Russo N, Himo F (2008) J Phys Chem B 112:2494–2500. doi:10.1021/jp710035j
24. Chen SL, Fang WH, Himo F (2007) J Phys Chem B 111:1253–1255. doi:10.1021/jp068500n
25. Bojin MD, Schlick T (2007) J Phys Chem B 111:11244–11252. doi:10.1021/jp071838c
26. InsightII, version 98.0 (1998) Accelrys Inc., San Diego
27. Frisch MJ, Trucks GW, Schlegel HB, Scuseria GE, Robb MA, Cheeseman JR, Montgomery JA Jr, Vreven T, Kudin KN, Burant JC, Millam JM, Iyengar SS, Tomasi J, Barone V, Mennucci B, Cossi M, Scalmani G, Rega N, Petersson GA, Nakatsuji H, Hada M, Ehara M, Toyota K, Fukuda R, Hasegawa J, Ishida M, Nakajima T, Honda Y, Kitao O, Nakai H, Klene M, Li X, Knox JE, Hratchian HP, Cross JB, Adamo C, Jaramillo J, Gomperts R, Stratmann RE, Yazyev O, Austin AJ, Cammi R, Pomelli C, Ochterski JW, Ayala PY, Morokuma K, Voth GA, Salvador P, Dannenberg JJ, Zakrzewski VG, Dapprich S, Daniels AD, Strain MC, Farkas O, Malick DK, Rabuck AD, Raghavachari K, Foresman JB, Ortiz JV, Cui Q, Baboul AG, Clifford J, Cioslowski J, Stefanov BB, Liu G, Liashenko A, Piskorz P, Komaromi I, Martin RL, Fox DJ, Keith T, AI-Laham MA, Peng CY, Nanayakkara A, Challacombe M, Gill PMW, Johnson B, Chen W, Wong MW, Gonzalez C, Pople JA (2003) Gaussian 03. Gaussian, Inc., Pittsburgh
28. Becke AD (1993) J Chem Phys 98:5648–5652. doi:10.1063/1.464913
29. Lee C, Yang W, Parr RG (1988) Phys Rev B 37:785–789. doi:10.1103/PhysRevB.37.785
30. Miehlich B, Savin A, Stoll H, Preuss H (1989) Chem Phys Lett 157:200–206. doi:10.1016/0009-2614(89)87234-3
31. Affinity User Guide (1999) Accelrys Inc., San Diego
32. O'Leary MH (1992) In: Sigman DS, Boyer PD (eds) The Enzymes 20:235–269, Academic Press, New York